J|A|C|S
ARTICLES

Published on Web 11/21/2008

Effects of the Arctic ($E^{22}\rightarrow G$) Mutation on Amyloid β-Protein Folding: Discrete Molecular Dynamics Study

A. R. Lam,[*,§,#] D. B. Teplow,[†] H. E. Stanley,[§] and B. Urbanc[‡,§]

Center for Polymer Studies, Physics Department, Boston University, Boston, Massachusetts 02215, Department of Neurology, David Geffen School of Medicine, and Molecular Biology Institute and Brain Research Institute, University of California, Los Angeles, California 90095, and Department of Physics, Drexel University, Philadelphia, Pennsylvania 19104

Received July 9, 2008; E-mail: arlam@buphy.bu.edu; alfonsol@ucr.edu

Abstract: The 40–42 residue amyloid β-protein (Aβ) plays a central role in the pathogenesis of Alzheimer's disease (AD). Of the two main alloforms, Aβ40 and Aβ42, the longer Aβ42 is linked particularly strongly to AD. Despite the relatively small two amino acid length difference in primary structure, *in vitro* studies demonstrate that Aβ40 and Aβ42 oligomerize through distinct pathways. Recently, a discrete molecular dynamics (DMD) approach combined with a four-bead protein model recapitulated the differences in Aβ40 and Aβ42 oligomerization and led to structural predictions amenable to *in vitro* testing. Here, the same DMD approach is applied to elucidate folding of Aβ40, Aβ42, and two mutants, [G22]Aβ40 and [G22]Aβ42, which cause a familial ("Arctic") form of AD. The implicit solvent in the DMD approach is modeled by amino acid-specific hydropathic and electrostatic interactions. The strengths of these effective interactions are chosen to best fit the temperature dependence of the average β-strand content in Aβ42 monomer, as determined using circular dichroism (CD) spectroscopy. In agreement with these CD data, we show that at physiological temperatures, the average β-strand content in both alloforms increases with temperature. Our results predict that the average β-strand propensity should decrease in both alloforms at temperatures higher than $\sim$370 K. At physiological temperatures, both Aβ40 and Aβ42 adopt a collapsed-coil conformation with several short β-strands and a small ($<$1%) amount of α-helical structure. At slightly above physiological temperature, folded Aβ42 monomers display larger amounts of β-strand than do Aβ40 monomers. At increased temperatures, more extended conformations with a higher amount of β-strand ($\lesssim$30%) structure are observed. In both alloforms, a β-hairpin at A21-A30 is a central folding region. We observe three additional folded regions: structure **1**, a β-hairpin at V36-A42 that exists in Aβ42 but not in Aβ40; structure **2**, a β-hairpin at R5-H13 in Aβ42 but not in Aβ40; and structure **3**, a β-strand A2-F4 in Aβ40 but not Aβ42. At physiological temperatures, the Arctic mutation, E22G, disrupts contacts in the A21-A30 region of both [G22]Aβ peptides, resulting in a less stable main folding region relative to the wild type peptides. The Arctic mutation induces a significant structural change at the N-terminus of [G22]Aβ40 by preventing the formation of structure **3** observed in Aβ40 but not Aβ42, thereby reducing the structural differences between [G22]Aβ40 and [G22]Aβ42 at the N-terminus. [G22]Aβ40 is characterized by a significantly increased amount of average β-strand relative to the other three peptides due to an induced β-hairpin structure at R5-H13, similar to structure **2**. Consequently, the N-terminal folded structure of the Arctic mutants closely resembles the N-terminal structure of Aβ42, suggesting that both Arctic Aβ peptides might assemble into structures similar to toxic Aβ42 oligomers.

1. Introduction

Alzheimer's disease (AD) is a progressive neurodegenerative disorder that is characterized pathologically by extensive neuronal loss and the accumulation of extracellular senile plaques and intracellular neurofibrillary tangles. Senile plaques contain fibrillar aggregates of the amyloid β-protein (Aβ). Aβ is produced through cleavage of the amyloid precursor protein (APP) and is normally present in the body predominantly in two alloforms, Aβ40 and Aβ42, that differ structurally by the absence or presence of two C-terminal amino acids, respectively.[1,2] An important hypothesis of disease causation, strongly supported by genetic and experimental evidence, posits that Aβ oligomers, rather than fibrils, are the proximate neurotoxic agents in AD.[3] In particular, Aβ42 oligomers appear to be the most toxic Aβ assemblies.[4] The linkage of Aβ oligomerization to AD makes imperative the detailed elucidation of the oligomerization process. Unfortunately, the Aβ system is remarkably complex

[#] Also affiliated with Department of Chemistry, 420 Chemical Sciences, University of California, Riverside, CA 92521.
[§] Boston University.
[†] University of California, Los Angeles.
[‡] Drexel University.

(1) Hardy, J.; Selkoe, D. J. *Science* **2002**, *297*, 353–356.
(2) Hardy, J. *Neurobiol. Aging* **2002**, *23*, 1073–1074.
(3) Roychaudhuri, R.; Yang, M.; Hoshi, M. M.; Teplow, D. B. *J. Biol. Chem.* **2008**, doi: 10.1074/jbc.R800036200.
(4) Dahlgren, K. N.; Manelli, A. M.; Stine, W. B.; Baker, L. K.; Krafft, G. A.; LaDu, M. J. *J. Biol. Chem.* **2002**, *277* (35), 32046–32053.

in its conformational and assembly dynamics.[3,5] This has complicated the application of classical structure determination methods such as X-ray crystallography and solution state NMR to the oligomerization question. One approach that has provided information on the initial self-association of Aβ has been *in situ* chemical cross-linking (for a review, see ref 6). This approach allowed Bitan *et al.*[7] to determine quantitatively the Aβ oligomer size frequency distribution, which demonstrated that Aβ40 and Aβ42 exhibit different oligomerization pathways. Aβ42 assembled into pentamer/hexamer units (paranuclei) and multiples of paranuclei, while Aβ40 only formed dimers through tetramers in equilibrium with monomers. However, the resolution of the method was insufficient to reveal the interatomic interactions controlling the oligomerization processes.

In vitro studies showed that Aβ40 and Aβ42 monomers adopted a predominantly α-helical structure in a membrane-mimicking environment,[8,9] while a collapsed coil structure was reported for Aβ(10–35) in an aqueous solution.[10] Aβ folded structure clearly depends on the solvent. Earlier studies of Aβ40 using a mixture of trifluoroethanol and water demonstrated a substantial amount of α-helical structure.[11,12] Initial studies of temperature dependence of the secondary structure of Aβ40 in aqueous solution demonstrated that β-strand propensity increased with temperature.[13] Using CD spectroscopy on both Aβ40 and Aβ42 monomers in aqueous solution, Lim *et al.* recently demonstrated[14] that the average β-strand structure increased with temperature, in agreement with Gursky and Aleshkov,[13] with Aβ42 monomers having a slightly higher amount of average β-strand structure than Aβ40 monomers, suggesting that the two alloforms are characterized by differences in folded structures.

Knowledge-based therapeutic drug design requires the definition of target structures at atomic resolution. *In silico* approaches provide a powerful means to achieve this goal. Several *in silico* studies addressed folding of Aβ42,[15,16] Aβ39,[17] Aβ(10–35),[18,19] Aβ(25–35),[20] Aβ(1–28),[21] and Aβ(21–30) decapeptide.[22−27] The latter was hypothesized to nucleate monomer folding.[28,29] Replica-exchange all-atom molecular dynamics (MD) study of Aβ42 monomer in implicit water by Baumketner *et al.* showed three distinct families of folded structures, all dominated by turns and loops with a small amount of α-helical structure at the C-terminus.[16] Using similar all-atom MD approach, Anand *et al.* found that at room temperature, the Aβ(1–39) monomer did not have a unique structure but rather three distinct families of mostly collapsed coil-like structures existed.[17] Using all-atom MD in explicit water, Massi *et al.* demonstrated that although Aβ(10–35) is somewhat disordered in water, the central hydrophobic cluster, L17-A21, and the turn region, V24-N27, were particularly stable.[18,19] Wei *et al.*[20] used replica-exchange MD in pure water and HFIP/water cosolvent to demonstrate that Aβ(25–35) preferentially populated an α-helical structure in apolar organic solvent, while in water, a collapsed coil, and to a lesser extent β-hairpin conformations, were observed. Dong *et al.*[21] explored the energy landscape of Aβ (1–28) monomers and concluded that the monomer was predominantly in a collapsed coil conformation with a non-negligible β-strand structure at the N-terminus.

An *ab initio* DMD approach using a four-bead protein model with backbone hydrogen bonding in implicit solvent recently demonstrated that despite relatively small differences in the primary structure, Aβ40 and Aβ42 not only followed different oligomerization pathways but also folded differently, with Aβ42 displaying a turn structure centered at G37-G38 that was not present in Aβ40 monomer.[30] This structural difference between Aβ40 and Aβ42 was corroborated by several independent *in vitro* studies.[28,31,32] In addition, a combined MD/NMR study confirmed that Aβ42 monomer was more structured at the C-terminus than Aβ40.[33] Using the same DMD approach as the initial study by Urbanc *et al.*,[30] Lam *et al.* showed that only selected regions of Aβ42 had a well-defined folded structure and that the average amount of β-strand increased with temperature,[34] consistent with *in vitro* findings.[13] Because Aβ40 and Aβ42 were shown to oligomerize through distinct pathways *in vitro*[7] and *in silico*,[30] the present study is based on a hypothesis that different oligomerization pathways leading to distinct effects *in vivo* are a consequence of folding differences between Aβ40 and Aβ42. We employ the DMD approach with

(5) Teplow, D. B. *Methods Enzymol.* **2006**, *413*, 20–33.
(6) Bitan, G.; Teplow, D. B. *Acc. Chem. Res.* **2004**, *37*, 357–364.
(7) Bitan, G.; Kirkitadze, M. D.; Lomakin, A.; Vollers, S. S.; Benedek, G. B.; Teplow, D. B. *Proc. Natl. Acad. Sci. USA* **2003**, *100*, 330–335.
(8) Coles, M.; Bicknell, W.; Watson, A. A.; Fairlie, D. P.; Craik, D. J. *Biochemistry* **1998**, *37*, 11064–11077.
(9) Crescenzi, O.; Tomaselli, S.; Guerrini, R.; Salvatori, S.; D'Ursi, A. M.; Temussi, P. A.; Picone, D. *Eur. J. Biochem.* **2002**, *269*, 5642–5648.
(10) Zhang, S.; Iwata, K.; Lachenmann, M. J.; Peng, J. W.; Li, S.; Stimson, E. R.; Lu, Y. A.; Felix, A. M.; Maggio, J. E.; Lee, J. P. *J. Struct. Biol.* **2000**, *130* (1), 130–141.
(11) Sticht, H.; Bayer, P.; Willbold, D.; Dames, S.; Hilbich, C.; Beyreuther, K.; Frank, R.; Rosch, P. *Eur. J. Biochem.* **1995**, *233*, 293–298.
(12) Fezoui, Y.; Teplow, D. B. *J. Biol. Chem.* **2002**, *277*, 36948–36954.
(13) Gursky, O.; Aleshkov, S. *Biochim. Biophys. Acta* **2000**, *1476*, 93–102.
(14) Lim, K. H.; Collver, H. H.; Le, Y. T. H.; Nagchowdhuri, P.; Kenney, J. M. *Biochem. Biophys. Res. Commun.* **2006**, *353*, 443–449.
(15) Bernstein, S. L.; Wyttenbach, T.; Baumketner, A.; Shea, J.-E.; Bitan, G.; Teplow, D. B.; Bowers, M. T. *J. Am. Chem. Soc.* **2005**, *127*, 2075–2084.
(16) Baumketner, A.; Bernstein, S. L.; Wyttenbach, T.; Bitan, G.; Teplow, D. B.; Bowers, M. T.; Shea, J.-E. *Protein Sci.* **2006**, *15*, 420–428.
(17) Anand, P.; Nadel, F. S.; Hansmann, U. H. E. *J. Chem. Phys.* **2008**, *128* (1–5), 165102.
(18) Massi, F.; Peng, J. W.; Lee, J. P.; Straub, J. E. *Biophys. J.* **2001**, *80*, 31–44.
(19) Massi, F.; Straub, J. E. *Biophys. J.* **2001**, *81*, 697–709.
(20) Wei, G. H.; Shea, J. E. *Biophys. J.* **2006**, *91* (5), 1638–1647.
(21) Dong, X.; Chen, W.; Mousseau, N.; Derreumaux, P. *J. Chem. Phys.* **2008**, *128* (1–10), 125108.
(22) Borreguero, J. M.; Urbanc, B.; Lazo, N.; Buldyrev, S. V.; Teplow, D. B.; Stanley, H. E. *Proc. Natl. Acad. Sci. USA* **2005**, *102*, 6015–6020.
(23) Cruz, L.; Urbanc, B.; Borreguero, J. M.; Lazo, N. D.; Teplow, D. B.; Stanley, H. E. *Proc. Natl. Acad. Sci. USA* **2005**, *102*, 18258–18263.
(24) W. Chen, N. M.; Derreumaux, P. *J. Chem. Phys.* **2006**, *125* (8), 084911.
(25) Baumketner, A.; Bernstein, S. L.; Wyttenbach, T.; Lazo, N. D.; Teplow, D. B.; Bowers, M. T.; Shea, J.-E. *Protein Sci* **2006**, *15*, 1239–1247.
(26) Krone, M. G.; Baumketner, A.; Bernstein, S. L.; Wyttenbach, T.; Lazo, N. D.; Teplow, D. B.; Bowers, M. T.; Shea, J.-E. *J. Mol. Biol.* **2008**,
(27) Tarus, B.; Straub, J. E.; Thirumalai, D. *J. Mol. Biol.* **2008**, *379* (4), 815–829.
(28) Lazo, N. D.; Grant, M. A.; Condron, M. C.; Rigby, A. C.; Teplow, D. B. *Protein Sci.* **2005**, *14* (6), 1581–1596.
(29) Grant, M. A.; Lazo, N. D.; Lomakin, A.; Condron, M. M.; Arai, H.; Yamin, G.; Rigby, A. C.; Teplow, D. B. *Proc. Natl. Acad. Sci. USA* **2007**, *104* (42), 16522–16527.
(30) Urbanc, B.; Cruz, L.; Yun, S.; Buldyrev, S. V.; Bitan, G.; Teplow, D. B.; Stanley, H. E. *Proc. Natl. Acad. Sci. USA* **2004**, *101*, 17345–17350.
(31) Murakami, K.; Irie, K.; Ohigashi, H.; Hara, H.; Nagao, M.; Shimizu, T.; Shirasawa, T. *J. Am. Chem. Soc.* **2005**, *127* (43), 15168–15174.
(32) Yan, Y.; Wang, C. *J. Mol. Biol.* **2006**, *364* (5), 853–862.
(33) Sgourakis, N. G.; Yan, Y.; McCallum, S. A.; Wang, C.; Garcia, A. E. *J. Mol. Biol.* **2007**, *368*, 1448–1457.
(34) Lam, A.; Urbanc, B.; Borreguero, J.; Lazo, N.; Teplow, D.; Stanley, H. E. *Proceedings of 2006 International Conference on Bioinformatics & Computational Biology* 2006, *1*, 322–328.

implicit solvent parameters mimicking the *in vitro* aqueous solution[14] to elucidate all structural differences between Aβ40 and Aβ42 monomers at different temperatures. Because the Arctic mutation, $E^{22}\rightarrow G$, is associated with the familiar form of AD with distinct pathology relative to the sporadic AD, we examine also the effects of the Arctic mutation on folded structures of both isoforms and discuss the implications of our findings for understanding Aβ isoform-specific folding and its relationship to AD.

2. Methods

2.1. Discrete Molecular Dynamics. Zhou *et al.* proposed the idea of applying discrete molecular dynamics (DMD) combined with a simplified protein model to study protein folding.[35] Since then, many groups have implemented this approach to investigate protein folding mechanisms.[36−40] In DMD, all interparticle interactions are modeled by square-well and step-like potentials. Particles move with constant speeds along straight lines. When two particles reach a distance at which the potential is discontinuous, a collision occurs. The pair of particles with the shortest collision time is chosen as the next collision event and the new positions and velocities of the two particles involved are calculated based on conservation laws for the linear momentum, angular momentum, and total energy. The advantage of DMD is that the numerical integration of Newton's second law equations is avoided, resulting in a substantial decrease in computational burden. This makes the DMD approach much faster than all-atom MD with continuous interparticle potentials.

2.2. Four-Bead Protein Model and Interactions. We use a four-bead protein model,[41−43] in which up to four beads are used to represent an amino acid. Three beads are used to model the backbone groups N, C_α, and C'. The fourth bead represents the side chain centered at the C_β group. Only glycine lacks the C_β bead and is thus modeled by three beads only. Adjacent beads are connected to each other through covalent or peptide bonds, which are modeled as square well potentials with infinite walls but of finite width corresponding to ∼2% variability in covalent/peptide bond lengths. In addition to covalent and peptide bonds, constraints are implemented to ensure the proper geometry of the protein backbone. These constraints are modeled in the same ways as the bonds. All lengths of bonds and constraints are based on statistical properties derived from the protein database of known protein structures.[44]

The backbone hydrogen bond was introduced into the four bead model to account for the α-helical and β-strand secondary structure.[43] The bond is introduced between the N_i bead of amino acid i and C'_j bead of amino acid j. For a hydrogen bond between N_i and C'_j to form, these two beads need to be at a distance <4.2 Å. In addition, auxiliary bonds between the two amino acids involved are introduced to account for the particular backbone geometry allowing hydrogen bond formation. The absolute value of the potential energy associated with formation of a single hydrogen bond, E_{HB}, represents a unit of energy in our approach. The simulation temperature T_{sim} is expressed in units of E_{HB}/k_B, where k_B is the Boltzmann constant.

The model implements amino acid-specific interactions between two side chain beads due to effective hydropathy[30] and charge.[34,44] The side chain bead of each amino acid is characterized by an effective hydropathy following the Kyte and Dolittle scale.[45] Because the solvent is not explicitly present in the model, effective attractive interactions between two hydrophobic, and repulsive interactions between two hydrophilic, side chain beads are introduced.[30,44] The strength of the effective hydropathic interactions as given by the absolute value of the potential energy between two isoleucines E_{HP} (relative to the energy unit E_{HB}) is the first interaction parameter. A double square-well potential is applied to model the effective electrostatic interactions between two charged side chain beads.[44] The maximal absolute value of the potential energy between two charged side chain beads E_{CH} (relative to the energy unit E_{HB}) is the second interaction parameter. Both interaction parameters E_{HP} and E_{CH} strongly depend on and need to be adjusted to the particular solvent.

2.3. Secondary Structure Analysis. The secondary structure propensities of each amino acid were calculated using the STRIDE program[46] within the Visual Molecular Dynamics (VMD) software package.[47] The secondary structure propensities included α-helical, β-strand, turn, and random coil per amino acid. We calculated the average β-strand and α-helix propensities, $\langle\beta\rangle$ and $\langle\alpha\rangle$, by averaging the β-strand/α-helix propensity over all amino acids at a given temperature and interaction parameters (E_{HP}, E_{CH}).

2.4. Intramolecular Contact Map. We determined the average intramolecular contact frequency for each temperature and interaction parameter set (E_{HP}, E_{CH}). Two amino acids, i and j, were considered to be in contact when the distance between them $d_{ij} \leq 7.5$ Å. The contact was counted with variable C_{ij} that was defined as the average number of contact pairs between amino acids i and j from different trajectories. Because each amino acid had up to four beads, the maximum number of contacts C_{ij} (between any two amino acids) was 16. We normalized the contact maps to the same maximum value.

3. Results

The DMD approach employed here has been described in detail by Urbanc *et al.*[44] In earlier studies, DMD combined with a four-bead amino acid model, and considering backbone hydrogen bonding only, resulted in β-hairpin monomer and planar dimer conformations.[48] Introducing amino acid-specific interactions due to hydropathy into the four-bead model enabled the successful *in silico* reproduction of experimentally observed[7] oligomerization differences between Aβ40 and Aβ42 and yielded new structural predictions amenable to *in vitro* testing.[30] This same study indicated that alloform-specific differences already existed at the stage of monomer folding. In particular, the turn structure centered at G37-G38 was present in a folded Aβ42 monomer but not in a folded Aβ40 monomer and was associated with the first contacts that formed during monomer folding. Yun *et al.*,[49] using the same DMD approach, showed that electrostatic interactions promote formation of larger oligomers in both Aβ40 and Aβ42 while preserving the

(35) Zhou, Y.; Hall, C. K.; Karplus, M. *Phys. Rev. Lett.* **1996**, *77*, 2822–2825.
(36) Zhou, Y. Q.; Karplus, M. *Proc. Natl. Acad. Sci. USA* **1997**, *94*, 14429–14432.
(37) Zhou, Y. Q.; Karplus, M.; Wichert, J. M.; Hall, C. K. *J. Chem. Phys.* **1997**, *107*, 10691–10708.
(38) Dokholyan, N. V.; Buldyrev, S. V.; Stanley, H. E.; Shakhnovich, E. I. *Folding Design* **1998**, *3*, 577–587.
(39) Zhou, Y. Q.; Karplus, M. *J. Mol. Biol.* **1999**, *293*, 917–951.
(40) Dokholyan, N. V.; Buldyrev, S. V.; Stanley, H. E.; Shakhnovich, E. I. *J. Mol. Biol.* **2000**, *296*, 1183–1188.
(41) Smith, A. V.; Hall, C. K. *Proteins: Struct. Funct. Genet.* **2001**, *4*, 344–360.
(42) Smith, A. V.; Hall, C. K. *J. Mol. Biol.* **2001**, *312*, 187–202.
(43) Ding, F.; Borreguero, J. M.; Buldyrev, S. V.; Stanley, H. E.; Dokholyan, N. V. *Proteins: Struct. Funct. Genet.* **2003**, *53*, 220–228.
(44) Urbanc, B.; Borreguero, J. M.; Cruz, L.; Stanley, H. E. *Methods Enzymol.* **2006**, *412*, 314–338.
(45) Kyte, J.; Doolittle, R. F. *J. Mol. Biol.* **1982**, *157*, 105–132.
(46) Heinig, M.; Frishman, D. *Nucleic Acids Res.* **2004**, *32*, W500–W502.
(47) Humphrey, W.; Dalke, A.; Schulten, K. *J. Mol. Graphics* **1996**, *14*, 33–38.
(48) Urbanc, B.; Cruz, L.; Ding, F.; Sammond, D.; Khare, S.; Buldyrev, S.; Stanley, H. E.; Dokholyan, N. V. *Biophys. J.* **2004**, *87* (4), 2310–2321.
(49) Yun, S. J.; Urbanc, B.; Cruz, L.; Bitan, G.; Teplow, D. B.; Stanley, H. E. *Biophys. J.* **2007**, *92* (11), 4064–4077.

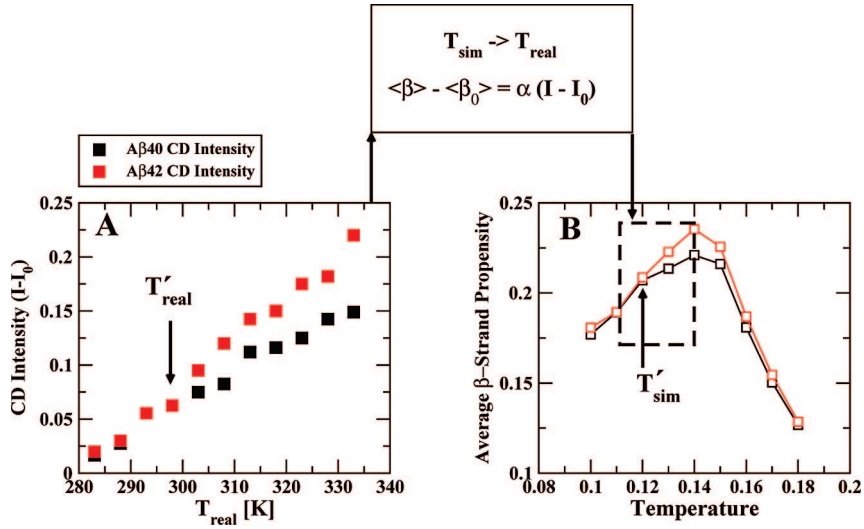

Figure 1. (A) CD data obtained for Aβ40 (black squares) and Aβ42 (red squares) by Lim *et al.*[14] (B) Average β-strand propensity, $\langle\beta\rangle$, of Aβ40 (black squares) and Aβ42 (red squares). For all the parameter sets (E_{HP}, E_{CH}), we map the CD data in panel **A** using the functions defined in the dashed-line box above the plot into the data enclosed in the dashed box in panel **B**. T_{sim}' and T_{real}' are related by a conversion factor ($T^* = T_{real}'/T_{sim}'$) that maps all the simulation temperatures onto real temperatures. A similar relationship exists for the CD intensity conversion factor α. $\langle\beta_0\rangle$ and I_0 are the average β-strand propensity and the CD intensity at 5 °C, respectively.

differences between the two alloforms at both the folding and oligomerization stages of assembly. Lam *et al.* applied this approach in studies of the temperature dependence of Aβ42 folding, showing that a collapsed coil conformation at low temperatures converts to a more extended, β-strand-rich conformation at higher temperatures.[34] Interestingly, while several regions of Aβ42 consistently exhibit a temperature-dependent fold, significant variability of folded structures was found at each temperature. The coexistence of a multitude of monomer conformations is characteristic of naturally unfolded proteins. Here we explore more deeply the differences between the full-length Aβ40 and Aβ42 peptides. We first describe a technique that allows us to determine the implicit solvent parameters that best match experimental conditions. We then use these parameters to explore not only the folding of wild type Aβ40 and Aβ42 but also of two clinically relevant mutant alloforms, Arctic [G22]Aβ40 and [G22]Aβ42.

The primary structure of Aβ42 differs from Aβ40 by two additional amino acids of Aβ42, I and A, at the C-terminus. The sequence of Aβ42 is DAEFRHDSGYEVHHQK^{16}LVFFAE^{22}DVGSNKGA^{30}IIGLMV^{36}GGVV^{40}IA. We refer to the segments (L17−A21) and (I31−V36) as the central hydrophobic cluster (CHC) and the mid-hydrophobic region (MHR), respectively. We define the C-terminal region (CTR) as the segment V39-V40 in Aβ40 or V39-V42 in Aβ42.

The energy unit is set to the absolute value of the hydrogen bond potential energy, $E_{HB} = 1.0$ and the simulation temperature T_{sim} is expressed in units of E_{HB}/k_B. We explore folding at four different strengths of hydropathic interactions, E_{HP}=0.1, 0.2, 0.3, 0.4, and three different strengths of EIs, $E_{CH} = 0$, 0.15, 0.3. For each set of these effective interaction parameters (E_{HP}, E_{CH}), we first perform DMD simulations of a monomer at a high temperature ($T_{sim} = 4$) to obtain 100 distinct random coil-like initial conformations to be used in production runs. For given interaction parameters (E_{HP}, E_{CH}), we simulate 100 trajectories spanning a temperature range of [0.10, 0.18].

3.1. Interaction Parameters for Aqueous Aβ Folding. In an aqueous environment, hydrophobic and hydrophilic effects play key roles in protein folding and assembly. In the DMD approach, we model hydropathic effects by a single-well attractive/repulsive potential between two side-chain beads. The strength of the effective hydropathic interactions, E_{HP}, is by definition equal to the absolute value of the potential energy between two I residues at a distance of <7.5 Å. Similarly, the strength of effective electrostatic interactions, E_{CH}, is defined as the absolute value of the potential energy between two oppositely charged side-chain atoms at a distance of <6 Å.

We examined the temperature dependence of Aβ40 and Aβ42 folding using 12 different sets of interaction parameters (E_{HP}, E_{CH}). Our goal was to select interaction parameters that would best fit the folded structure of Aβ in aqueous solution. As an input, we used the *in vitro* data by of Lim *et al.*,[14] who applied CD spectroscopy to characterize the secondary structure of Aβ40 and Aβ42 monomers in a broad temperature range (Fig. 1A). The resulting CD intensities for Aβ40 and Aβ42 increased linearly with temperature T_{real} and above $T_{real}' = 298$ K, the CD intensity for Aβ42 surpassed the Aβ40 intensity, indicating a higher $\langle\beta\rangle$ in Aβ42 for $T_{real} > T_{real}'$.

At given interaction parameters (E_{HP}, E_{CH}), we calculated the average β-strand propensity, $\langle\beta\rangle$, for each Aβ40 and Aβ42, which could be compared to the CD intensities. Our *in silico* results for $\langle\beta\rangle$ for both Aβ40 and Aβ42 were in agreement with the CD data obtained by Lim *et al.* (Fig. 1B). At low temperatures, $\langle\beta\rangle$ in both peptides increased with temperature linearly, and above the temperature T_{sim}', Aβ42 had more β-strand structure than Aβ40.

Assuming that $\langle\beta\rangle$ was proportional to the CD intensity, we fitted the calculated temperature dependence of $\langle\beta\rangle$ for Aβ42 monomer to the temperature dependence of the CD intensity. For each set of interaction parameters (E_{HP}, E_{CH}), we first determined the simulation temperature T_{sim}', above which $\langle\beta\rangle$ of Aβ42 was larger than $\langle\beta\rangle$ of Aβ40. We matched T_{sim}' to T_{real}' to obtain the temperature scaling factor T^* (eq 1),

$$T^* = T_{real}'/T_{sim}' \quad (1)$$

and used T^* to scale the simulation temperature T_{sim} to the real temperature T_{real}.

CD spectroscopy provides a rapid method for the determination of the population average secondary structure frequency

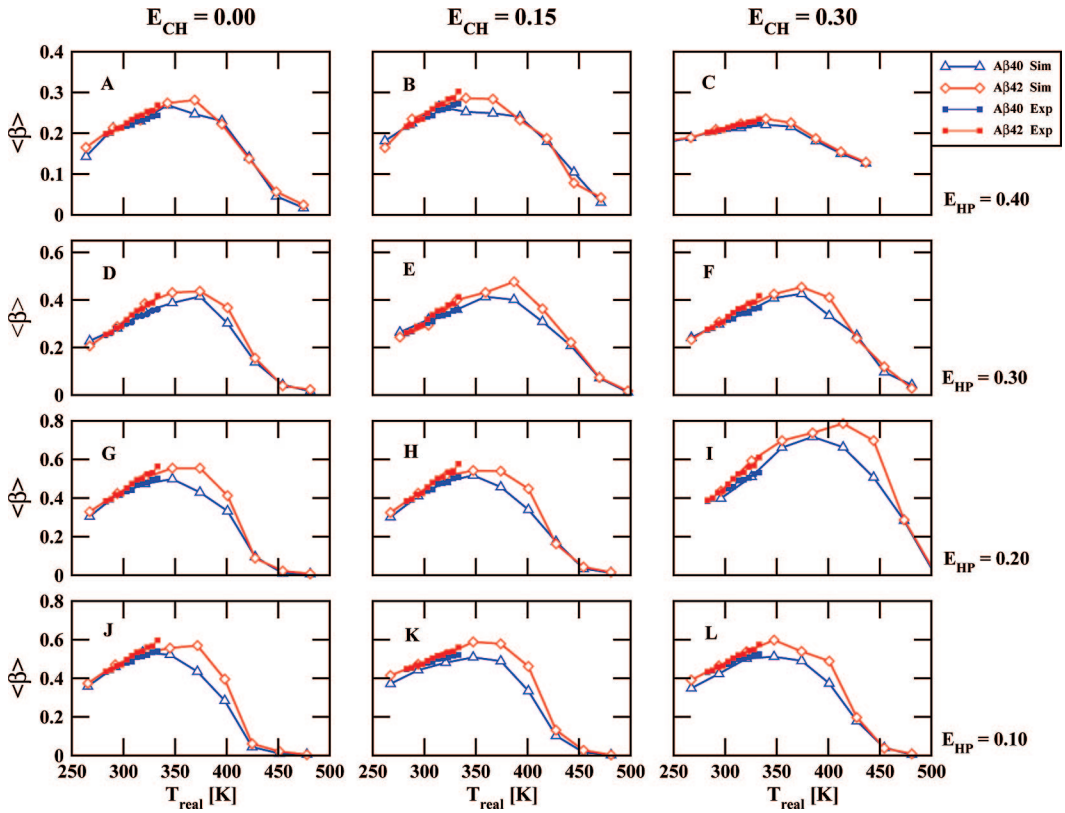

Figure 2. Average β-strand propensity, $\langle\beta\rangle$, versus temperature for all the elements of the parameter matrix (E_{HP}, E_{CH}). The graphs with empty blue triangles and empty red diamonds correspond to the Aβ40 and Aβ42 simulations, respectively. Similarly for the CD data, blue and red filled squares correspond to Aβ40 and Aβ42 experimental points, respectively.

distribution. In a recent paper, Greenfield suggested that a linear relationship exists between CD intensity and the sum of the secondary structure elements contributing to it.[50] To relate the average β-strand propensity $\langle\beta\rangle$ derived from our simulations to CD intensities I_{CD} determined experimentally, we used the data of Lim *et al.*[14] These data were obtained at 222 nm, not at ~218 nm, where the minimum in β-strand ellipticity occurs. Nevertheless, because the β-strand is the dominant secondary structure element in our Aβ monomer conformations and because $\theta_{218} \propto \theta_{222}$, $\langle\beta\rangle$ will be proportional to CD intensity at 222 nm. We thus relate the CD intensity data, $I_{CD}-I_0$ (the y-axis of Fig. 2C in ref 14), to the calculated $\langle\beta\rangle$ using the following equation:

$$\langle\beta\rangle - \langle\beta_0\rangle = \alpha(I_{CD} - I_0) \qquad (2)$$

where $\langle\beta_0\rangle$ was $\langle\beta\rangle$ at 5 °C (278 K) and I_0 was the corresponding CD intensity at 5 °C. The scaling factor α was obtained by fitting I_{CD} to $\langle\beta\rangle$.

For all sets of interaction parameters (E_{HP}, E_{CH}), the physiological temperature was found to be within the simulation temperature range $T_{sim} \in [0.11, 0.12]$ (Fig. 2).

We fitted $\langle\beta\rangle$ of the folded Aβ42 monomer to the CD intensities for 12 different sets of interaction parameters (E_{HP}, E_{CH}). Once the two fitting parameters, T^* and α, were obtained we used them to calculate $\langle\beta\rangle$ versus temperature not only for Aβ42 but also for Aβ40. For each interaction parameter set (E_{HP}, E_{CH}), we quantified the quality of the fit, including temperature dependencies of $\langle\beta\rangle$ for both Aβ40and Aβ42, by calculating σ:

$$\sigma = \sqrt{\frac{1}{(N-1)\cdot\langle\beta\rangle_{max}^{\ 2}} \sum (\langle\beta\rangle_{exp} - \langle\beta\rangle_{sim})^2} \qquad (3)$$

(50) Greenfield, N. J. *Nature Protocols* **2007**, *1*, 2876–2890.

Table 1. Calculation of σ To Determine the Quality of the Fitting[a]

	E_{CH}		
E_{HP}	0.00	0.15	0.30
0.10	0.0459	0.0898	0.0734
0.20	0.0387	0.0490	0.0682
0.30	0.0461	0.0690	0.0478
0.40	0.0596	0.0440	*0.024*

[a] The parameter set (E_{HP}, E_{CH}) that best fit the CD data was (0.40, 0.30) (in italics).

where N is the number of experimental temperatures at which the CD intensity was measured, $\langle\beta\rangle_{max}$ is the highest value of $\langle\beta\rangle$ in the simulation data set, $\langle\beta\rangle_{exp}$ is the experimental value of $\langle\beta\rangle$ obtained from fitting the CD intensities to $\langle\beta\rangle$ (eq 2), and $\langle\beta\rangle_{sim}$ corresponds to the value of $\langle\beta\rangle$ obtained by simulations and interpolated to exactly match the temperatures at which the CD intensities were measured. σ values for each interaction parameter set (E_{HP}, E_{CH}) are listed in Table 1.

Examining the effect of varying the strengths of the two effective interaction parameters, we observed that $\langle\beta\rangle$ decreased with increasing E_{HP} but showed only minor changes with increasing E_{CH}. For $E_{HP} \in [0.1, 0.2]$, $\langle\beta\rangle$ did not change significantly (Fig. 2G-L). Increasing E_{CH} from 0 to 0.15 at $E_{HP} = 0.2$ did not change $\langle\beta\rangle$ in either of the two peptides. However, at $E_{CH} = 0.3$ (Fig. 2I), $\langle\beta\rangle$ amounts in both peptides were higher than the amounts observed at $E_{CH} \in [0, 0.15]$ but they followed the experimentally observed tendencies: $\langle\beta\rangle_{42} > \langle\beta\rangle_{40}$. $\langle\beta\rangle$ strongly decreased when E_{HP} changed from 0.2 to 0.3 (Fig. 2D-I). Variations in E_{CH} did not significantly affect $\langle\beta\rangle$ at $E_{HP} = 0.3$. When E_{HP} increased from 0.3 to 0.4 (Fig. 2A-F), we observed a further decrease of $\langle\beta\rangle$ at all temperatures in both peptides while preserving the experimentally observed differ-

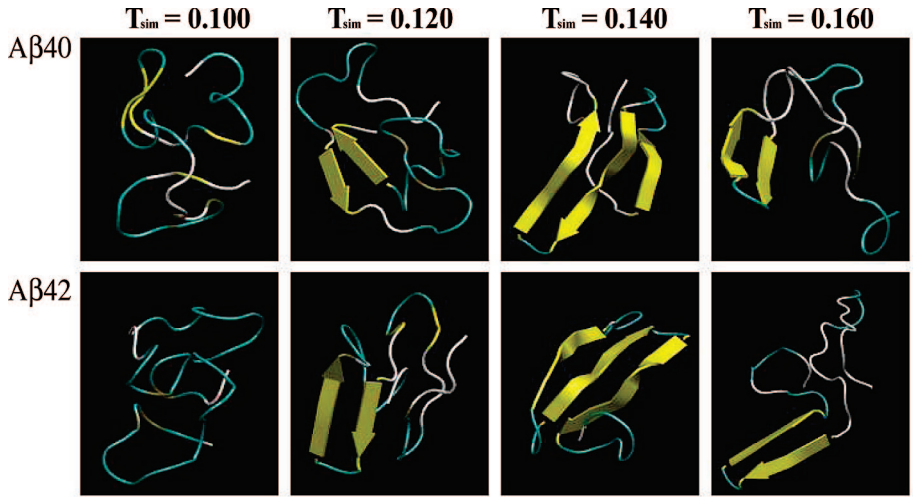

Figure 3. Typical conformations of Aβ40 (top) and Aβ42 (bottom) at different temperatures.

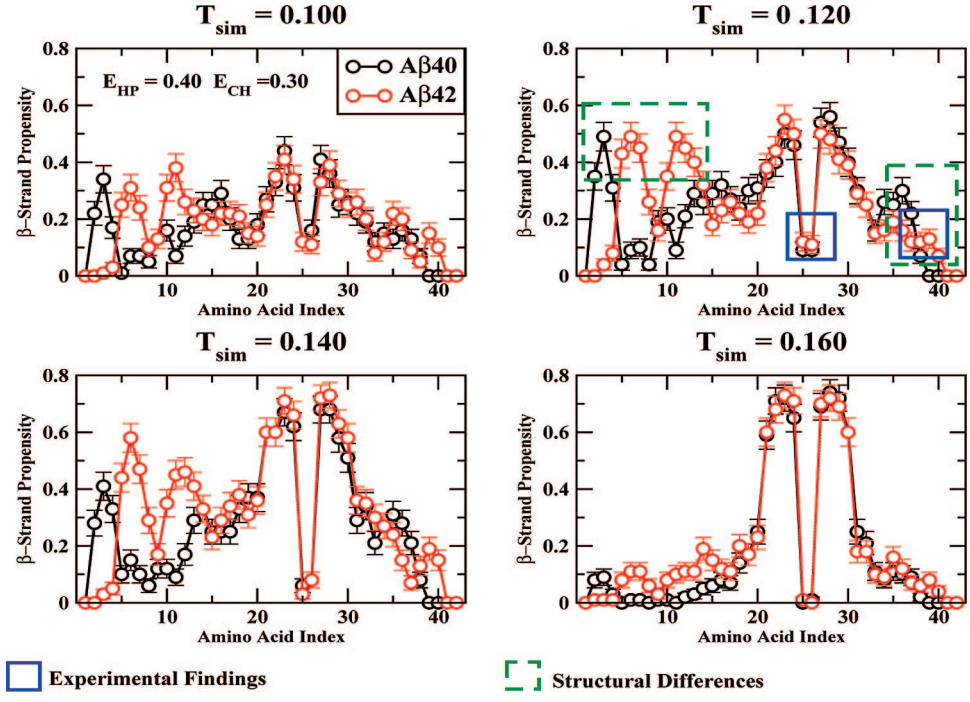

Figure 4. Amino acid-specific β-strand propensities for Aβ40 (black) and Aβ42 (red) at four different temperatures using the parameter set (0.40, 0.30). Differences in the termini between Aβ peptides are highlighted by the dashed-line boxes. The solid-line boxes show the turn/loop centered at G25-S26 and G37-G38 observed experimentally.[28,31,32]

ences in $\langle\beta\rangle$ between the two alloforms. At $E_{HP} = 0.4$ (Fig. 2A-C), increase in E_{CH} from 0 to 0.3 resulted in a decrease of $\langle\beta\rangle$ at all temperatures in both peptides.

In the following, we used the interaction parameters that best matched the experimental data, $E_{HP} = 0.4$ and $E_{CH} = 0.3$, to characterize the structural differences in Aβ40 and Aβ42 monomer folding at different temperatures. The physiological temperature $T_{real} = 310$ K was found to correspond to the simulation temperature $T_{sim} = 0.124$.

3.2. Aβ40 and Aβ42 Folded Structures Differ. Fig. 3 shows "typical" folded structures of both peptides at four selected temperatures. We define "typical" as a conformation that possesses the average amount of β-strand structure that strongly increases with temperature. At a fixed temperature, a large variability in the conformational space of folded Aβ monomers has been observed in our own previous study[34] and by others.[16,33] With increasing temperatures, a larger number of β-strand-rich conformations were observed. At high temperatures, thermal fluctuations destroy any secondary structure and result in random-coil conformations. Similar conformational transitions in a mixture of monomers and dimers in aqueous solution were reported by Gursky and Aleshkov.[13] To gain more detailed structural information, we calculated amino acid-specific β-strand propensities (Fig. 4) and constructed intramolecular contact maps. These maps show the pairwise amino acid interaction frequencies, thereby allowing identification of peptide regions contributing significantly to folding (Fig. 5).

Fig. 4 shows that all β-strand propensities were below 40% at $T_{sim} = 0.1$, increased with temperature, reached the highest values of up to 80% at $T_{sim} = 0.14$, and decreased at yet higher temperatures. At the physiological temperature $T_{sim} = 0.12$, the regions with the highest β-strand propensities were A2-F4 (Aβ40

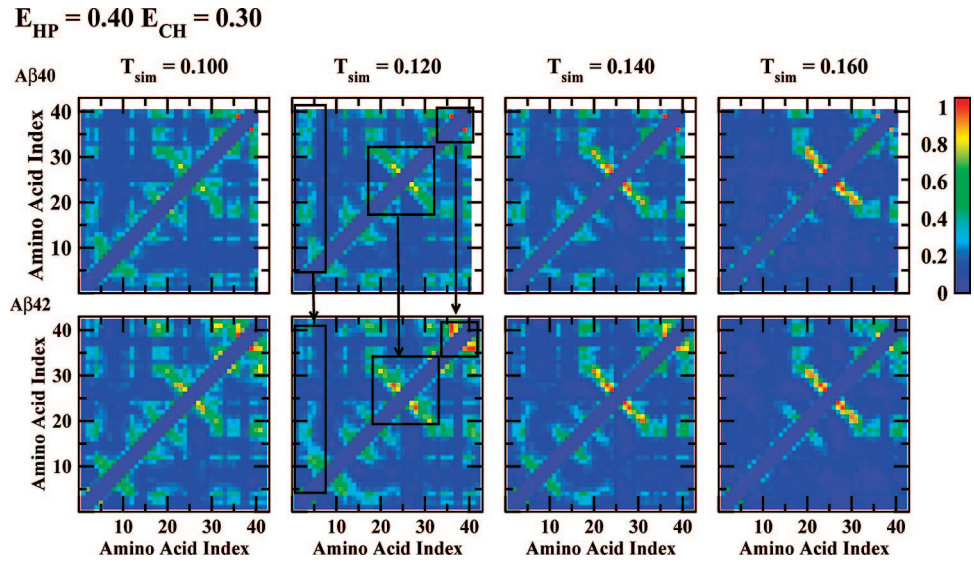

Figure 5. Intramolecular average contact maps of Aβ40 (upper) and Aβ42 peptides (lower) at different temperatures and $E_{HP} = 0.40$ and $E_{CH} = 0.30$. The axes are numbered according to amino acid position, where 1 is the N-terminus. The pairwise contact frequency is represented by color (see scale at right). The boxes within the maps of Aβ40 and Aβ42 at $T_{sim} = 0.120$ highlight the differences between these two peptides.

only), R5-D7 and Y10-V12 (Aβ42 only), F21-V24, N27-G29, and the MHR (Aβ40 and Aβ42), and the CTR (Aβ42 only). Fig. 5 shows that the largest number of contacts in both alloforms was observed *between* the CHC and MHR. This central folding region which was hypothesized by Lazo *et al.*[28] to nucleate the folding, was associated with a turn centered at G25-S26 that was bounded by extended strands at F21-V24 and N27-G29.

The contacts between the MHR and CTR were significantly stronger in Aβ42 than in Aβ40. In Aβ42, the strength of these contacts surpassed that of the central folding region. These contacts were associated with a turn centered at G37-G38 in Aβ42, but not in Aβ40. The existence of a folded structure at the CTR of Aβ42 is supported by a non-zero β-strand propensity ($\approx$10%). In contrast, the CTR of Aβ40 displays zero β-strand propensity. The existence of this turn structure in Aβ42 was observed initially by Urbanc *et al.*[30] and confirmed *in vitro* by several experimental groups.[28,31,32]

The region A2-F4 had a high β-strand propensity in Aβ40 but not in Aβ42 (40% at $T_{sim} = 0.1$, 50% at $T_{sim} = 0.12$, and >40% at $T_{sim} = 0.14$). The number of contacts formed between the segment A2-F4 and other parts of the peptide also was larger in Aβ40 than in Aβ42 (Fig. 5). The segments R5-D7 and Y10-V12 exhibited increased β-strand propensities in Aβ42 (>30% at $T_{sim} = 0.1$, $\approx$50% at $T_{sim} = 0.12$, and >40% at $T_{sim} = 0.14$). These two segments formed a β-hairpin centered at S8-Y10 in Aβ42. This hairpin occurs significantly less frequently in Aβ40, in which the entire segment R5-Q15 shows a significantly smaller β-strand propensity ($\leq$20%) at all temperatures than does the equivalent segment in Aβ42 (Fig. 4). Lim *et al.* reported temperature-induced changes at the N-terminal region of Aβ40 and Aβ42 that may be important for their amyloidogenic properties.[14] However, the N-terminal (A2-Q15) structural differences between Aβ40 and Aβ42 were not observed so far.

We next calculated the average α-helix propensity, $\langle\alpha\rangle$, at each simulation temperature T_{sim}. At the physiological temperature, $T_{sim} = 0.12$, $\langle\alpha\rangle$ was 0.1% for Aβ40 and 0% for Aβ42. At lower temperatures, $\langle\alpha\rangle$ was 0% and 0.3%, respectively. At $T_{sim} = 0.1$, $\langle\alpha\rangle = 0.3\%$ in Aβ40 and $\langle\alpha\rangle = 0.1\%$ in Aβ42. At temperatures above the physiological temperature, $\langle\alpha\rangle$ was 0% in both Aβ40 and Aβ42 (data not shown).

3.3. Effect of the Arctic ($E^{22}\rightarrow G$) Mutation on Aβ Folding. We explored here the effects of the clinically relevant Arctic mutation[51] on Aβ folding. *In vitro* studies have determined that [G22]Aβ40 has a higher propensity to form protofibrils than does Aβ but that the overall rate of fibril formation remains constant.[51] A recent study by Grant *et al.*[29] showed that the Arctic mutation significantly destabilized the turn structure in the central folding region A21-A30.

We used the optimal interaction parameters $E_{HP} = 0.4$ and $E_{CH} = 0.3$ in our simulations. Fig. 6A shows $\langle\beta\rangle$ over a wide temperature range for Aβ40, Aβ42, [G22]Aβ40, and [G22]Aβ42. The temperature dependence of $\langle\beta\rangle$ for Arctic peptides followed the same trend as Aβ. At low temperatures, $\langle\beta\rangle$ increased gradually until it reached a maximum at $T_{sim} = 0.14$. For T_{sim} >0.14, $\langle\beta\rangle$ decreased.

As described above, $\langle\beta\rangle$ in Aβ increased with temperature in both alloforms and at $T_{sim} > 0.11$, the average β-strand propensity of Aβ42, $\langle\beta\rangle_{42}$ surpassed the average β-strand propensity of Aβ40, $\langle\beta\rangle_{40}$. In contrast, in the Arctic mutants in the same temperature range, $\langle\beta\rangle_{[G22]40} > \langle\beta\rangle_{[G22]42}$ (Fig. 6A). As shown in Fig. 6A, at $T_{sim} \in [0.11, 0.15]$, $\langle\beta\rangle$ of [G22]Aβ40 (blue line with squares) was larger than that of Aβ40 (black line with circles) by 3–5%, while $\langle\beta\rangle$ in [G22]Aβ42 was 2–3% larger than in Aβ42.

Important structural differences between [G22]Aβ40 and [G22]Aβ42 were observed in the calculated β-strand propensities per amino acid (Fig. 6B). At a physiological temperature, $T_{sim} = 0.12$, both alloforms showed similar β-strand propensities in the segment F21-V24 (50%), whereas the β-strand propensity of the segment N27-G29 was significantly larger in [G22]Aβ40 (50%) than in [G22]Aβ42 (35%). Overall, the β-strand propensities in the central folding region of Aβ40, Aβ42, and [G22]Aβ40 were comparable. In the intramolecular contact map

(51) Nilsberth, C.; Westlind-Danielsson, A.; Eckman, C. B.; Condron, M. M.; Axelman, K.; Forsell, C.; Stenh, C.; Luthman, J.; Teplow, D. B.; Younkin, S. G.; Naslund, J.; Lannfelt, L. *Nature Neuro.* **2001**, *4* (9), 887–893.

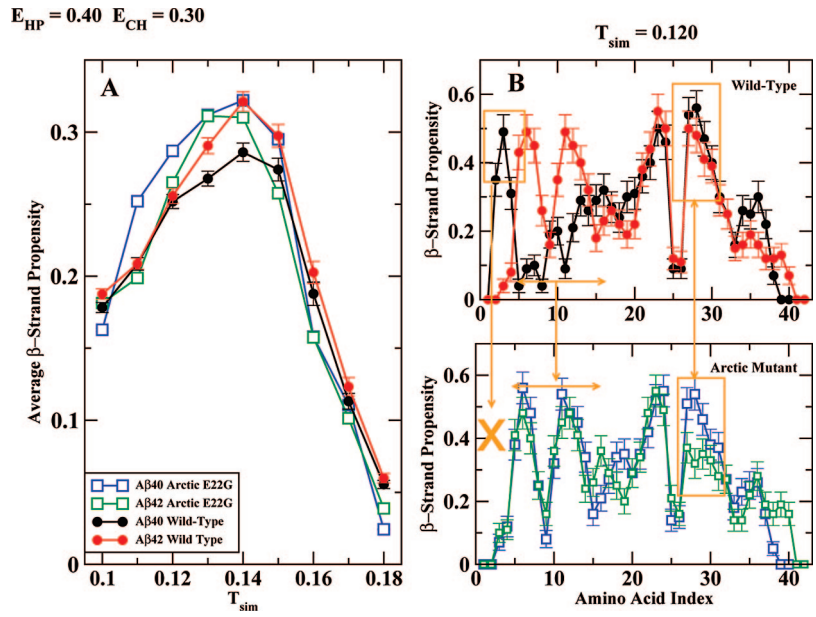

Figure 6. (A) The average β-strand propensity of [G22]Aβ (solid lines with empty squares; blue for [G22]Aβ40 and green for [G22]Aβ42) and Aβ (solid lines with filled circles; black for Aβ40 and red for Aβ42) at different temperatures. (B) Amino acid-specific β-strand propensity at $T_{sim} = 0.120$ for Aβ (top) and [G22]Aβ (bottom) peptides with parameters $E_{HP} = 0.40$ and $E_{CH} = 0.30$. The boxes indicate the structural differences between wild type and Arctic peptides. The yellow X indicates the substantial differences between the N-termini of the two peptides.

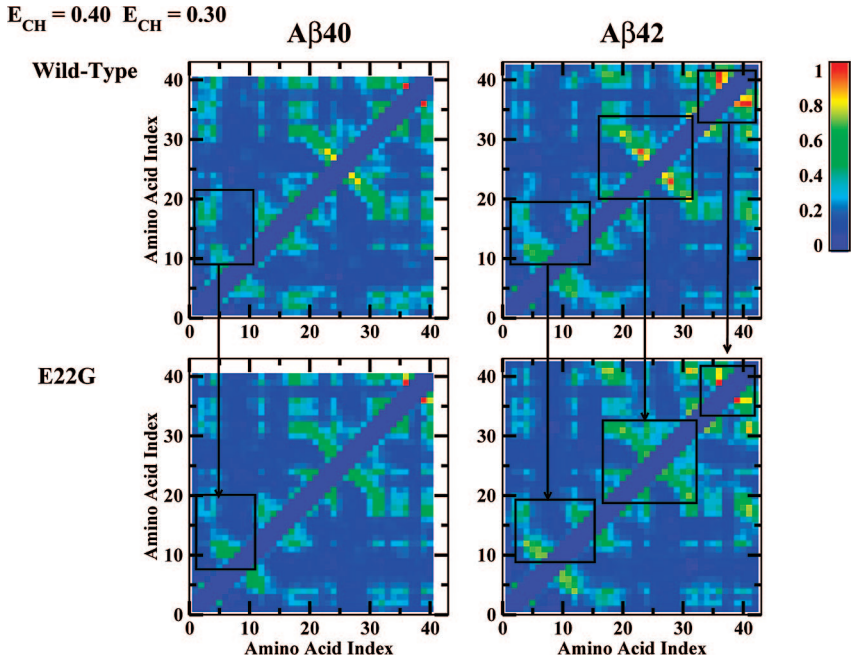

Figure 7. Intramolecular contact maps for Aβ (top) and [G22]Aβ (bottom) peptides with parameters $E_{HP} = 0.40$ and $E_{CH} = 0.30$ at $T_{sim} = 0.120$. The black boxes highlight differences in contact frequency between segments of wild type (top) and Arctic mutant (bottom) peptides.

corresponding to the Arctic mutants, decreased numbers of contacts were observed in the central folding region of both [G22]Aβ40 and [G22]Aβ42 relative to Aβ40 and Aβ42 (Fig. 7), suggesting that the Arctic mutation destabilizes the central folding region as also observed *in vitro* for the decapeptide Aβ (21–30) by Grant *et al.*[29]

At the N-terminus, the β-strand propensity of the segment R5-Q15 (Fig. 6B, top and bottom) was similar in [G22]Aβ40, [G22]Aβ42, and Aβ42, while in Aβ40, no significant β-strand propensity was associated with this region. The β-strand propensity of the segment A2-F4 was small (10%) and similar in both Arctic peptides, similar to Aβ42 but in contrast to that same region in Aβ40, where the β-strand propensity was 40–50%. The segments R5-D7 and Y10-V12 in [G22]Aβ40 had β-strand propensities >50%, compared to only slightly reduced propensity ($\approx$47%) in [G22]Aβ42. In both Arctic peptides, as well as in Aβ42, these two segments form a β-hairpin centered at S8-Y10.

In [G22]Aβ42, the β-strand propensity of the CTR was 20% higher than that in Aβ42, however, the intramolecular contact map shows a slightly decreased number of contacts in this region, suggesting that the Arctic mutation induced a confor-

(52) Han, W.; Wu, Y. D. *J. Am. Chem. Soc.* **2005**, *127* (44), 15408–15416.

Table 2. Hydrogen Bonds Appearing Most Frequently in Aβ and [G22]Aβ peptides[a]

segment	HB pair	Aβ40	[G22]Aβ40	Aβ42	[G22]Aβ42
TR1	F20:D23	5 ± 0.62	10 ± 1.27	4 ± 0.49	7 ± 0.88
	E22:G29	9 ± 1.14	3 ± 0.35	10 ± 1.27	5 ± 0.62
	V24:N27	31 ± 3.69	33 ± 3.89	31 ± 3.69	21 ± 2.60
TR2	V36:V39	11 ± 1.40	12 ± 1.52	5 ± 0.62	6 ± 0.75
NTR	R5:S8	11 ± 1.40	3 ± 0.35	2 ± 0.22	0
	R5:V12	1 ± 0.10	4 ± 0.49	4 ± 0.49	10 ± 1.27
	D7:Y10	3 ± 0.35	20 ± 2.48	14 ± 1.77	20 ± 2.48
	S8:E11	1 ± 0.10	13 ± 1.65	19 ± 2.37	13 ± 1.65
	H13:K16	14 ± 1.77	15 ± 1.89	8 ± 1.02	8 ± 1.02

[a] The numbers are percent (%) occurrence ± the standard errors.

mational change in the CTR from a more collapsed into a more extended structure. The turn structure centered at G37-G38 was observed in [G22]Aβ42 but not in [G22]Aβ40 (data not shown). [G22]Aβ40 did not show any β-strand propensity in the CTR region (Fig. 6B, bottom). Consistent with this result, the CTR of [G22]Aβ42 had a larger number of contacts with the MHR (Fig. 7, right column), relative to Aβ42. In the MHR, both Arctic peptides exhibited similar β-strand propensity (>20%). Here, we observed that the MHR of [G22]Aβ42 had higher β-strand propensity than Aβ42. Comparing the intramolecular contact maps of [G22]Aβ and Aβ at a physiological temperature $T_{sim} = 0.120$, we found an increased number of contacts between the MHR and CTR in [G22]Aβ42 relative to [G22]Aβ40. [G22]Aβ40 had less contacts between the N-terminus and the CHC relative to Aβ40 (Fig. 7).

3.4. The Role of Hydrogen Bonding in Aβ Folding. We examined the backbone hydrogen bonds formed in Aβ and [G22]Aβ at the physiological temperature $T_{sim} = 0.120$. We determined the percentage of hydrogen bonds present in three important segments: F20-I31 (central folding region TR1), V36-V39 (C-terminal folding region TR2), and R5-K16 (N-terminal folding region, NTR). The hydrogen bond formation propensity in these segments was lower than suggested by the β-strand propensities per amino acid (Fig. 6B). The most frequent backbone hydrogen bonds are listed in Table 2.

In all four peptides, the central folding region TR1 was associated with the highest hydrogen bond propensity. In Aβ40, the hydrogen bonds F20:D23 and E22:G29 appeared in 5% and 9% conformations, respectively, and the hydrogen bond V24:N27 appeared in 31% conformations. In [G22]Aβ40, the hydrogen bond F20:D23 appeared in 10% of conformations while the propensity of the hydrogen bond E22:G29 decreased to 3%. The hydrogen bond V24:N27 in [G22]Aβ40 had an increased frequency of 33% with respect to the wild type (21%). In Aβ42, the hydrogen bond F20:D23 had low hydrogen bond propensities of 4% while E22:G29 and V24:N27 had propensities of 10% and 31%, respectively. These propensities decreased in [G22]Aβ42 to 7%, 5%, and 21%.

The hydrogen bond in the TR2 region V36:V39 was formed with 11% propensity in Aβ40 and with 5% in Aβ42 conformations. In [G22]Aβ40 and [G22]Aβ42, the TR2 showed an increase 12% and 6%, respectively.

In the N-terminal folding region NTR, there were five relevant hydrogen bonds: R5:S8, R5:V12, D7:Y10, S8:E11, and H13:K16. In Aβ40, the backbone hydrogen bonds R5:S8 and H13:K16 were present with the highest propensities at 11% and 14%, respectively, while R5:V12 (1%), D7:Y10 (3%), and S8:E11 (1%) were present with low propensities. In Aβ42 the hydrogen bonds with the highest propensities D7:Y10 with 14% and S8:E11 with 19%. R5:S8, R5:V12, and H13:K16 had low propensities of 2%, 4%, and 8%, respectively. The Arctic peptide [G22]Aβ40 was characterized by hydrogen bonds D7:Y10 with 20%, S8:E11 with 13%, and H13:K16 with 15%, while R5:S8 and R5:V12 ended with 3% and 4%, respectively. In [G22]Aβ42 only the hydrogen bonds R5:V12, D7:Y10, and S8:E11 were present, with 10%, 20%, and 13% propensities, respectively. Here, R5:S8 was absent and H13:K16 remained with propensity of 8%. These results indicate that the Arctic mutation increased the propensity for backbone hydrogen bond formation with respect to wild type peptides. However, the pattern of the backbone hydrogen bonds in [G22]Aβ40 and [G22]Aβ42 was consistent with a β-hairpin structure at R5:Q15 similar to the one in Aβ42.

4. Conclusions

In this paper we examined folding of full-length Aβ40 and Aβ42, and their Arctic mutants, using DMD combined with a four-bead protein model and implicit solvent interactions. The temperature-induced conformational transitions obtained *in silico* were consistent with *in vitro* experiments that showed conformational transitions from a collapsed coil at low temperatures to a β-strand-rich extended conformations at higher temperatures.[13] Consistent with the CD measurements by Lim *et al.*,[14] we observed a faster increase of the average amount of β-strand in Aβ42 relative to Aβ40. Our model predicted the central folding region centered at G25-S26 in both Aβ40 and Aβ42, and the C-terminal folded structure centered at G37-G38 in only Aβ42, in agreement with *in vitro* findings of several groups.[28,31,32]

Existing experimental[10] and all-atom MD[18,52,53] studies on the fragment Aβ(10–35) are consistent with our observation of the collapsed coil monomer structure dominated by loops, bends, and turns at low temperatures. Our results demonstrate that small changes in the primary structure can have significant impact on folding, suggesting that full-length Aβ40 and Aβ42 and their mutants need to be examined to gain insights into pathological differences between the alloforms. The present study extends our understanding of how the additional amino acids I^{41} and A^{42} at the CTR of Aβ42 significantly impact full-length Aβ folding. The more hydrophobic CTR of Aβ42 is known to facilitate structural changes resulting in different oligomerization pathways and pathologies of Aβ40 and Aβ42. Bitan *et al.*[7] reported that Aβ40 forms smaller oligomers (from dimers to tetramers) while Aβ42 forms larger oligomers (pentamers/hexamers) and their multiples. Our studies demonstrate that structural differences between Aβ40 and Aβ42 that mediate this distinct oligomerization behavior already exist in the isolated peptide monomers. The structural difference between the two alloforms at the C-terminus, a turn centered at G37-G38 in Aβ42 but not in Aβ40, seems to be a direct consequence of two additional hydrophobic amino acids at the C-terminus of Aβ42. However, the folding differences between Aβ40 and Aβ42 at the N-termini, the β-strand at A2-F4 in Aβ40 but not in Aβ42 as well as a β-hairpin centered at S8-Y10 in Aβ42 but not in Aβ40, were surprising. This structural difference at the N-terminus of Aβ40 versus Aβ42 has not been reported experimentally, to our knowledge. Hou *et al.*[54] studied Aβ with reduced and oxidized M35 and showed that a turn or bend-like structure at D7-E11 in oxidized peptides was less frequent than

(53) Baumketner, A.; Shea, J. E. *J. Mol. Biol.* **2007**, *366* (1), 275–285.

in the redox peptides. As the structure at the N-terminal region was suggested to impact the amyloidogenic properties of Aβ,[14] the structural difference between the two alloforms reported here might provide a new clue to understanding oligomerization differences between Aβ40 and Aβ42.

Examining folding of the two Arctic mutants, [G22]Aβ40 and [G22]Aβ42, we showed that the presence of Gly^{22} disrupts contacts close to position 22, and importantly, also at the N-terminus of Aβ40, resulting in a [G22]Aβ40 conformer that is structurally similar to Aβ42 in this region. The average amount of β-strand formed at a physiological temperature in [G22]Aβ40 is higher than in [G22]Aβ42. Our observation that the substitution E22G increases the propensity for β-strand formation is not surprising. This substitution not only reduces the overall negative charge of the Arctic peptides but also, through the G^{22} substituent, increases the local backbone flexibility needed for a collective hydrogen bond ordering into a β-strand. In our study, the Arctic mutation did not significantly alter the structure of Aβ42. Instead, the major effect appeared to be on the secondary structure of Aβ40, which was more "Aβ42-like". The increased level of regular secondary structure in Aβ40 is likely to affect its oligomerization pathway, as observed *in vitro* and *in vivo*.[4,55,56]

Several studies have reported that the Arctic mutation significantly increases the protofibril formation rate relative to the wild type.[51,57] Our simulation result for [G22]Aβ40 shows an increase in the average β-strand propensity when compared to the wild type, which is consistent with these experimental findings. Dahlgren *et al.*[4] developed two aggregation protocols for the production of stable oligomeric or fibrillar preparations of Aβ42 and its Dutch ($E^{22}\rightarrow$Q) and Arctic mutants. In terms of neurotoxicity, the wild type and the mutants were not significantly different, but they observed extensive protofibril and fibril formation by the mutant peptides. Experimental studies by Murakami *et al.* demonstrated that the mutations at positions 22 and 23 played a significant role in Aβ assembly.[58] Specifically, the Arctic mutant showed a 50% increase in the average β-strand content in Aβ oligomers. Whalen *et al.* found that Arctic Aβ had an increased rate of assembly into oligomers and that these oligomers were more toxic to neurons in culture than were wild type oligomers.[59] These experimental findings on Arctic peptides are consistent with the increased β-strand propensity in folded Arctic monomers relative to their wild type counterparts. Take together with other data extant, our results suggest that small changes in the primary structure of Aβ not only may affect peptide monomer folding itself but also the rate of formation, structure, and neurotoxic properties of higher order assemblies.

Acknowledgment. This work was supported by the NIH program project grant AG023661. The work at Boston University was also supported by the Alzheimer Association through the award of a Zenith Award, and by a gift from Stephen Bechtel. D.B.T. acknowledges support from NIH grant AG027818, as well as the Jim Easton Consortium for Alzheimer's Drug Discovery and Biomarkers at UCLA and the State of California Alzheimer's Disease Research Fund (#07-65806).

JA804984H

(54) Hou, L. M.; Shao, H. Y.; Zhang, Y. B.; Li, H.; Menon, N. K.; Neuhaus, E. B.; Brewer, J. M.; Byeon, I. J. L.; Ray, D. G.; Vitek, M. P.; Iwashita, T.; Makula, R. A.; Przybyla, A. B.; Zagorski, M. G. *J. Am. Chem. Soc.* **2004**, *126* (7), 1992–2005.

(55) Cheng, I. H.; Palop, J. J.; Esposito, L. A.; Bien-Ly, N.; Yan, F. G.; Mucke, L. *Nature Med.* **2004**, *10* (11), 1190–1192.

(56) Cheng, I. H.; Scearce-Levie, K.; Legleiter, J.; Palop, J. J.; Gerstein, H.; Bien-Ly, N.; Puolivali, J.; Lesne, S.; Ashe, K. H.; Muchowski, P. J.; Mucke, L. *J. Biol. Chem.* **2007**, *282* (33), 23818–23828.

(57) Johansson, A. S.; Berglind-Dehlin, F.; Karlsson, G.; Edwards, K.; Gellerfors, P.; Lannfelt, L. *FEBS* **2006**, *273* (12), 2618–2630.

(58) Murakami, K.; Irie, K.; Morimoto, A.; Ohigashi, H.; Shindo, M.; Nagao, M.; Shimizu, T.; Shirasawad, T. *Biochem. Biophys. Res. Commun.* **2002**, *294*, 5–10.

(59) Whalen, B. M.; Selkoe, D. J.; Hartley, D. M. *Neurobiology of Disease* **2005**, *20*, 254–266.